Front. Struct. Civ. Eng. 2025, 19(3): 341–357
https://doi.org/10.1007/s11709-025-1132-4

RESEARCH ARTICLE

Investigation on lateral seismic isolation system of a typical long-span single-tower cable-stayed bridge for mountainous areas

Shichun ZHANG[a], Junjun GUO[a], Wei LIU[a], Jibo LI[b], Zhongguo GUAN[a*]

[a] *State Key Laboratory of Disaster Reduction in Civil Engineering, Tongji University, Shanghai 200092, China*
[b] *China Highway Engineering Consulting Co., Ltd., Beijing 100089, China*
[*] *Corresponding author. E-mail: guanzhongguo@tongji.edu.cn*

© Higher Education Press 2025

ABSTRACT This study focuses on a reasonable lateral isolation system for a typical long-span single-tower cable-stayed bridge with a significantly asymmetric span arrangement that is particularly suitable for mountainous areas. Based on the Jinsha River Bridge, the significant structural asymmetry and its effects on structural seismic responses were analyzed. The significantly asymmetric characteristics could result in complex dynamic behavior in seismic conditions and the lateral seismic responses of the structure are governed by multiple modes. A multilinear model composed of an ideal elastoplastic element and a multilinear elastic element was used to simulate different hysteresis, and a parametric analysis was conducted to investigate the appropriate damping hysteresis for the lateral seismic isolation of such a bridge. It shows that the inverted S-shaped hysteresis has relatively smaller secant stiffness and could help to balance the great difference in the lateral stiffness of the tower/piers. Thus, the inverted S-shaped hysteresis could lead to more efficient damping effects and less base shear forces of the tower/piers. A correlation between the reasonable yield forces of the dampers in the lateral isolation system, determined through an influence matrix-based method, and the shear forces of the corresponding bearings in the lateral fixed system was also observed. Moreover, the influence of geological conditions including different terrain and site conditions on the reasonable lateral isolation system was further investigated. It suggests to use dampers at all tower/pier locations when the side span crosses a steep valley slope, while a lateral isolation system without using dampers at the auxiliary piers could be employed when the side span crosses a gentle valley slope. Soft sites require larger damper yield forces and cause greater seismic responses compared to hard sites.

KEYWORDS single-tower cable-stayed bridge, lateral isolation system, multilinear model, influence matrix, geological conditions

1 Introduction

In recent years, there has been a growing demand for transportation infrastructure in the central and western regions of China. For bridges spanning the deep valleys in those mountainous areas with a main span ranging from 200 to 400 m, a typical long-span single-tower cable-stayed bridge with a steel−concrete hybrid girder could provide a superior aesthetic and economical solution. Up to now, a number of such single-tower cable-stayed bridges have been built in the central and western regions, as shown in Table 1. The span arrangement of this bridge is noticeably asymmetric, with a large length ratio between the main span and the side span, allowing for the maximization of the main span length and the construction of the tower on the side slope rather than the valley bed. However, the frequent occurrence of strong earthquakes in those regions poses a significant challenge to those bridges.

The lateral movement of the girder of a cable-stayed bridge under service loads usually needs to be constrained at the tower/pier locations. However, this system would cause significant seismic responses on the towers, piers, and foundations, so it is only applicable for bridges in

Article history: Received Dec 25, 2023; Accepted May 15, 2024

Table 1 Asymmetric single-tower cable-stayed bridges built in central and western China

Bridge	Year	Location	Span arrangement (m)
Yuekou Hanjiang River Bridge	2017	Hubei, China	32.7 + 50 + 93.7 + 260 + 38.2
New Yuehu Bridge	2018	Hubei, China	232 + 70 + 40 + 20
The Sixth Tuojiang River Bridge	2018	Sichuan, China	55 + 200 + 58 + 50
Yazuiyan Bridge	2019	Hunan, China	200 + 74 + 45
Xiangluzhou Bridge	2024	Hunan, China	300 + 180
Jinsha River Bridge	2024	Yunnan, China	340 + 72 + 48 + 32

low seismicity conditions [1]. In the case of a severe seismic action, it is often necessary to utilize appropriate damping devices for lateral seismic isolation of the bridges. Xie and Sun [2] investigated the influence of lateral viscous dampers on the seismic performance of a cable-stayed bridge in the transverse direction with a focus on the damper arrangement, and analyzed the reasonable damping coefficients of the dampers with the control variates method [3]. Xu et al. [4] and Ye and Fan [5] analyzed the influence of a lateral sliding system, a lateral fixed system, and a lateral isolation system with viscous dampers on the seismic response of the super-long-span cable-stayed bridge based on the Sutong Yangtze River Highway Bridge, and determined the appropriate damper parameters and arrangement with the parameter sensitivity analysis method [6]. Since viscous dampers cannot provide the anticipated lateral constraints under service loads, supplementary "sacrificial" limiting devices are needed. Nevertheless, the impact effect generated at the moment of failure of the "sacrificial" limiting devices during an earthquake event might significantly amplify the displacement response of the viscous dampers [1]. Mild steel damper is a typical displacement-dependent energy dissipation device and has been widely used for structural seismic isolation [7–12]. Camara and Astiz [13] compared two lateral isolation systems using viscous dampers and steel dampers. With a performance limit of critical cracking of concrete at the bottom of the tower of the cable-stayed bridge, an approximate method based on an equivalent single-degree-of-freedom system was proposed to determine the optimal damping parameters of the dampers [14]. Shen et al. [15–17] presented a new type of triangular steel damper for transverse shock absorption of side piers of a cable-stayed bridge, and the reasonable design parameters of the dampers were determined by using the exhaustive method [18] with the assistance of numerical software programming. Xu et al. [19,20] discussed the influence of different design parameters and arrangement forms of C-shaped steel dampers on the lateral damping effect of the cable-stayed bridge, and proposed a parameter design method based on equal yielding strength analysis. Wen et al. [21] explored the optimal parameters of the triangular steel dampers of the lateral isolation system for a long-span cable-stayed bridge with the genetic algorithm based on parallel computation. Niu et al. [22] proposed a simplified design method for the design of lateral isolation system with steel dampers of the cable-stayed bridge by taking displacement response as the control target. Based on a practical bridge, He et al. [23] and Wang et al. [24] studied the damping effect of steel dampers for seismic alleviation of the cable-stayed bridge in the transverse direction, and determined the optimal damper parameters using the parameter sensitivity analysis method [6]. Guan et al. [25] proposed a new lateral isolation system consisting of elastic or elastoplastic cables and a parallel viscous damper at the girder-tower connections for the seismic control of the Yongning Yellow River Bridge with a heavyweight concrete girder in the high seismic region [26,27], where the reasonable design parameters of the new system were also determined by the parameter sensitivity analysis method [28].

However, most of the preceding studies focused on the typical cable-stayed bridges with two towers and a symmetric span arrangement [25–30]. These bridges usually exhibit superior structural seismic performance, allowing for a reduction in the number of parameter variables for dampers in the lateral isolation system due to their structural symmetry. Little attention has been paid to the typical single-tower cable-stayed bridge, which is particularly suitable for mountainous areas with a significantly asymmetric span arrangement. This asymmetric design tends to induce highly intricate seismic behavior involving certain unexpected torsional movement when subjected to lateral loads. Therefore, the corresponding lateral isolation system should be well-matched with the asymmetric characteristics and accommodate the seismic actions effectively.

In this paper, based on a long-span single-tower cable-stayed bridge with a hybrid girder, namely the Jinsha River Bridge, the significant asymmetry and seismic response characteristics of the structure were analyzed. A multilinear model that can well simulate the hysteretic relationships of different displacement-dependent dampers was proposed to determine the reasonable damping hysteresis, and an influence matrix-based method was used to calculate the reasonable damper parameters. Furthermore, the influence of different terrain and site conditions on the reasonable lateral isolation system of

the single-tower cable-stayed bridge was further discussed.

2 Structural model and dynamic characteristics

2.1 Bridge description

The Jinsha River Bridge, depicted in Fig. 1, is a single-tower cable-stayed bridge with a steel–concrete hybrid girder. With a total length of 492 m, this bridge has a main span of 340 m and a span arrangement of (340 + 72 + 48 + 32) m. The hybrid girder has a typical cross-section of 32.3 m wide and 3.5 m high, as shown in Fig. 2(a). More specifically, the main span adopts a steel box girder, while the side span utilizes a concrete box girder with additional weight between the 5# and 6# piers to balance the asymmetric span arrangement. The heights of two transition piers (2# and 6#) and two auxiliary piers (4# and 5#) are 68.90, 21.93, 45.11, and 31.22 m, respectively. The diamond-shaped tower, depicted in Fig. 2(b), stands at a height of 197.6 m and comprises two columns connected by upper and lower beams to enhance its transverse stiffness. There are 40 pairs of cables attached to the tower with a spacing of 2.5 to 3.0 m and supporting the girder with a spacing of 4.5 to 16 m, forming a space fan-shaped double-cable plane. A total of

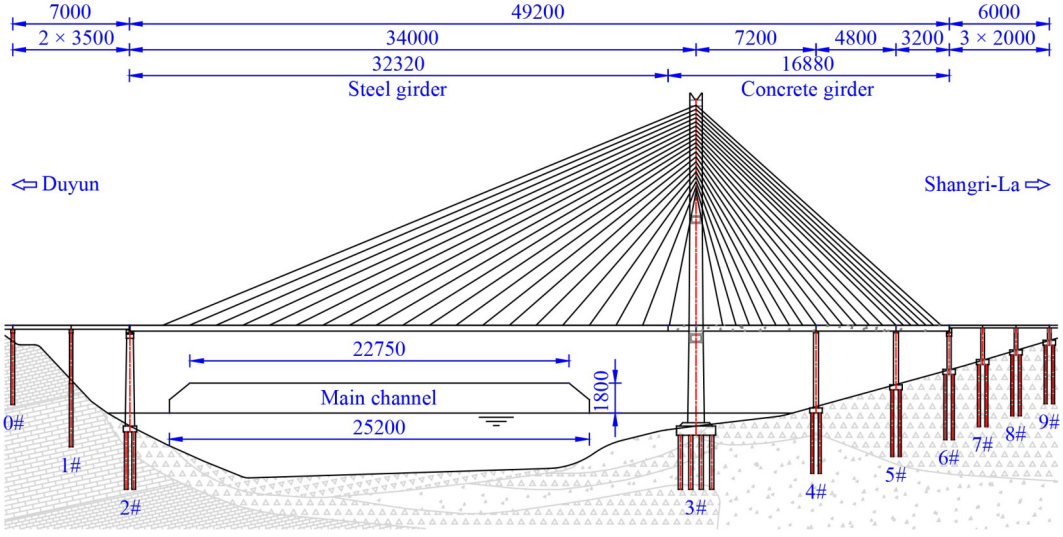

Fig. 1 Elevation of the cable-stayed bridge (unit: cm).

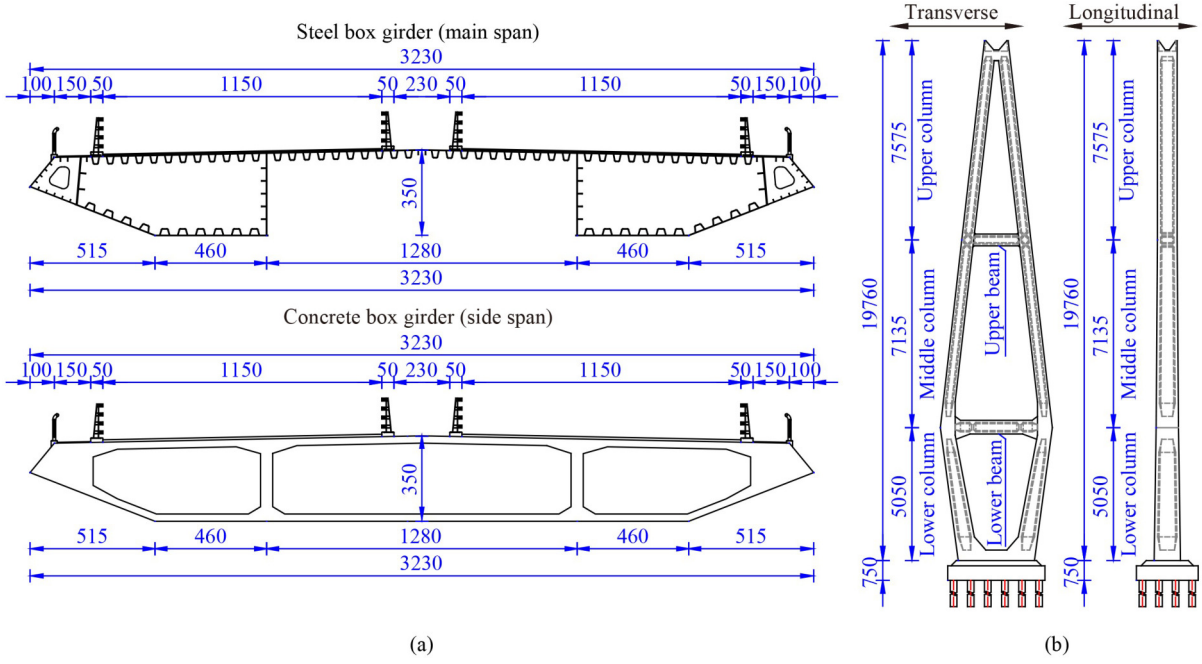

Fig. 2 Configuration of girder and tower (unit: cm): (a) hybrid girder; (b) diamond-shaped tower.

ten sliding bearings installed on the lower beam of the tower and the tops of the piers allow free movement of the girder in the longitudinal direction. All piers and the tower are supported by group-pile foundations consisting of cast-in-place piles, which are 40 to 75 m in length and 1.8 to 2.5 m in diameter.

2.2 Seismic action

Given the vital role of the cable-stayed bridge in the local transportation network, it is imperative for the structure to maintain elasticity even under a Level II earthquake that has a 2500-year return period. The response spectrum (5% damping) for the Level II earthquake was developed by the Institute of Crustal Dynamics of China Earthquake Administration (ICDCEA) based on the site survey, as illustrated in Fig. 3(a). The peak ground acceleration (PGA) is 0.311*g*, and the maximum acceleration of the spectrum is 0.871*g* within the period range of 0.1 to 0.8 s.

Four earthquake time-history records were selected from the NGA-West2 ground motion database of the Pacific Earthquake Engineering Research Center [31], as detailed in Table 2, and three artificial ground motions were generated by the ICDCEA. Figure 3(a) presents the response spectra corresponding to these artificial ground motions and earthquake records, indicating that they are compatible with the design response spectrum. Figure 3(b) illustrates the acceleration time histories of one artificial ground motion and one earthquake record. Since this study primarily focuses on the transverse seismic responses, a uniaxial excitation with these ground motions in the transverse direction was applied to the analyzed bridge only. Note that the seismic responses presented are the average results obtained from these seven ground motions.

2.3 Finite element model

A three-dimensional finite-element model of the Jinsha River Bridge was developed using the SAP2000 program. So far, a few physical models tested on shaking tables have been conducted for cable-stayed bridges. Those tests provided essential verification and useful guidance for the rational finite element models of such complicated structures [32,33]. With the guidance, the girder, tower, and piers were modeled as elastic beam elements. The additional weight, deck pavement and guardrails were represented as distributed loads along the girder. Note that the variations of the axial forces in the cables under the seismic action did not exceed the tension forces caused by the gravity load, which prevented the cables from becoming slack, and thus the cables were modeled as elastic truss elements with an equivalent elastic modulus considering the sag effect [34]. Nonlinear geometric (P-Delta) effects were included in the analysis as well. Moreover, the sliding bearings were modeled using Plastic Wen units to consider the coulomb friction, which is important during the interaction between the superstructure and substructure [35,36]. In the lateral fixed system, the fixed constraints in the transverse direction between the girder and tower/piers were represented as elastic link elements with substantial

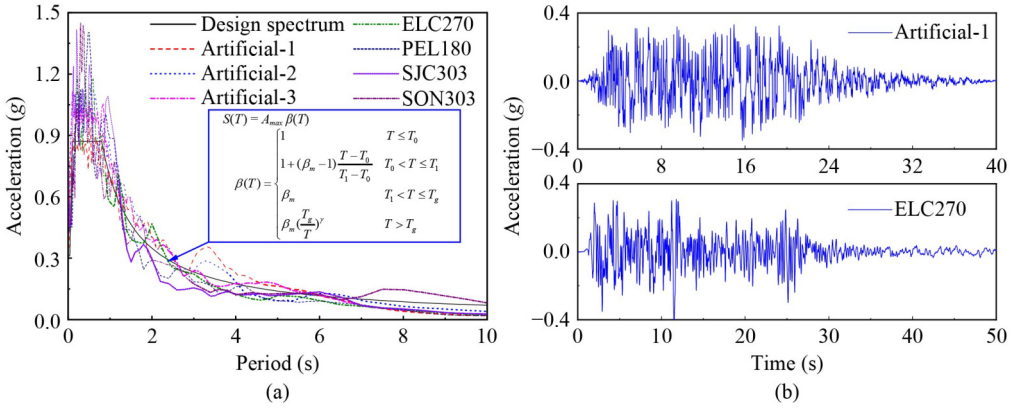

Fig. 3 Ground motion input: (a) acceleration response spectra (5% damping); (b) acceleration time histories.

Table 2 Selected earthquake records

Event	Year	Station, component	Magnitude	R_{rup} (km)	Duration (s)
Imperial Valley-02	1940	El Centro Array #9, ELC270	6.95	6.09	53.45
Kern County	1952	LA-Hollywood Stor FF, PEL180	7.36	117.75	139.99
San Fernando	1971	San Juan Capistrano, SJC303	6.61	108.01	98.80
San Fernando	1971	San Onofre-So Cal Edison, SON303	6.61	124.79	104.93

Note: R_{rup} represents the distance from the fault rupture surface to the site.

stiffness. Each pile group was simulated as a spring element with 6 × 6 degrees of freedom at the bottom center of the pile cap. The spring properties were calculated using the m method presented in the code JTG 3363-2019 [37]. In addition, the adjacent approach bridges were also included to consider their influence on the transition piers of the main bridge. The entire finite element model is depicted in Fig. 4.

2.4 Structural asymmetry and its effects on dynamic characteristics

As mentioned previously, the Jinsha River Bridge has a significantly asymmetric span arrangement. The length ratio of the side span to the main span is approximately equal to 0.45, which is relatively uncommon and fairly small among the existing bridges. To achieve a balanced weight distribution between the side span and the main span, the steel-concrete hybrid girder was adopted. The distributed mass of the concrete girder segment (side span) is approximately 5.28 times that of the steel girder segment (main span), as shown in Fig. 5. Moreover, the additional weight was added to the girder between the 5# and 6# piers in the bridge to further enhance the weight balance.

The terrain of the valley also leads to different heights of the piers, with the one closest to the tower being the tallest and those farther away being shorter. This results in significant asymmetry in the lateral stiffness distribution of the substructures. As depicted in Fig. 5, the tower provides the largest stiffness for lateral constraint of the girder, which is about 2.51 times that of the 6# pier and 30.55 times that of the 4# pier. Notably, the figure reveals that the center of substructural stiffness and the center of superstructural mass do not coincide.

Figure 6(a) presents the transverse cumulative modal participating mass ratios of the first 100 modes of the Jinsha River Bridge in the traditional lateral fixed system, i.e., the girder is fixed at all tower/pier locations in the transverse direction. It shows that the sum of the modal participating mass ratios of the 3rd, 8th, 10th, 15th, and 57th modes is approximately 85%. Figure 6(b) displays the shapes of the 3rd, 8th, and 10th modes. It can be seen that the 3rd mode shape is a combination of the transverse bending motion of the girder, primarily in the main span, and the lateral bending motion of the tower. The 8th and 10th modes exhibit similar asymmetric transverse motions of the main span, while those of the side span are in the opposite direction.

Figure 7 depicts the transverse displacement response of the girder for each mode under the design response spectrum. In addition, the displacement responses computed from the combination of the first 100 modes and the combination of three primary modes (the 3rd, 8th, and 10th modes) using the complete quadratic combination method [38] are also shown in the figure. As can be seen from the figure, the displacement response obtained from the combination of the first three transverse main modes is essentially consistent with that of the first 100 modes. This indicates that these three modes govern the transverse displacement response of the girder. In contrast, the 15th and 57th modes contribute minimally to the displacement response of the girder, although they have large modal participating mass ratios. More specifically, the 3rd mode primarily controls most of the main span and the portion of the side span near the tower, while the 8th and 10th modes have significant influence on the portion near the two ends, i.e., near the 2# and 6# transition piers.

Table 3 displays the accelerations of the girder, shear

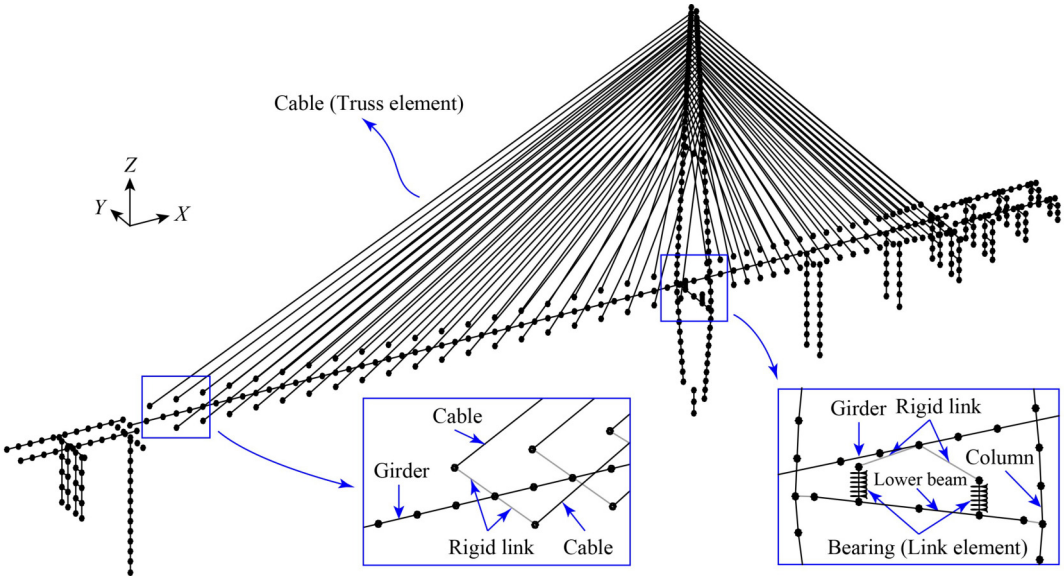

Fig. 4 Finite element model of the cable-stayed bridge.

forces of the bearings, and base shear forces of the tower/piers of the Jinsha River Bridge in the lateral fixed system, which exhibit significant variations from one position to another.

The above analysis shows that the single-tower cable-stayed bridge with a hybrid girder has significant asymmetry in span arrangement, mass distribution, and lateral stiffness of the tower/piers. The transverse seismic responses of the structure are dominated by multiple modes, and quite uneven seismic responses are induced at different tower/pier locations. This implies that meticulous consideration is necessary in designing an effective lateral isolation system for such a bridge.

3 Reasonable damping hysteresis for lateral isolation system

As mentioned previously, the tower and piers of a cable-stayed bridge should provide necessary restraints to the girder to prevent excessive lateral displacements under service loads, while sufficient relative deformation and energy dissipation are expected between the tower/piers and the girder under seismic actions. Displacement-dependent dampers have elastoplastic or similar constitutive properties. With appropriate design parameters, these dampers could remain elastic under service loads and yield during an earthquake event. This ensures that the distinct requirements for restraining the girder are well satisfied.

Different types of displacement-dependent dampers exhibit distinct constitutive relationships. The widely used friction pendulum isolation bearings provide a typical parallelogram-shaped hysteresis, which can be considered as the combination of a linear elastic link providing restoring capability and a coulomb friction for energy dissipation [39–41]. Wan et al. [42] have proposed a new displacement-dependent damper comprising a

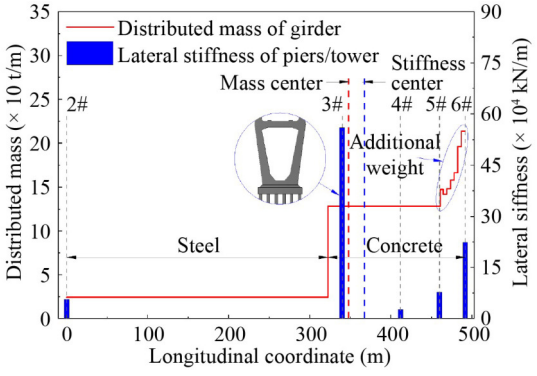

Fig. 5 Distribution of girder mass and substructural lateral stiffness.

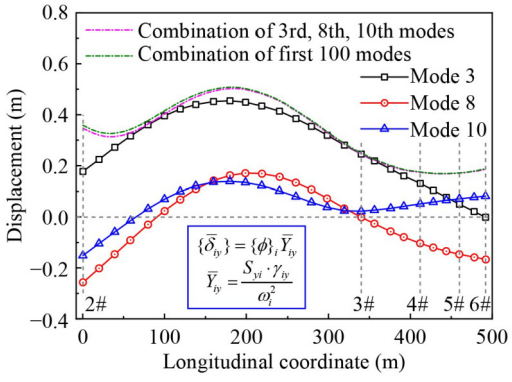

Fig. 7 Girder displacements for different transverse modes.

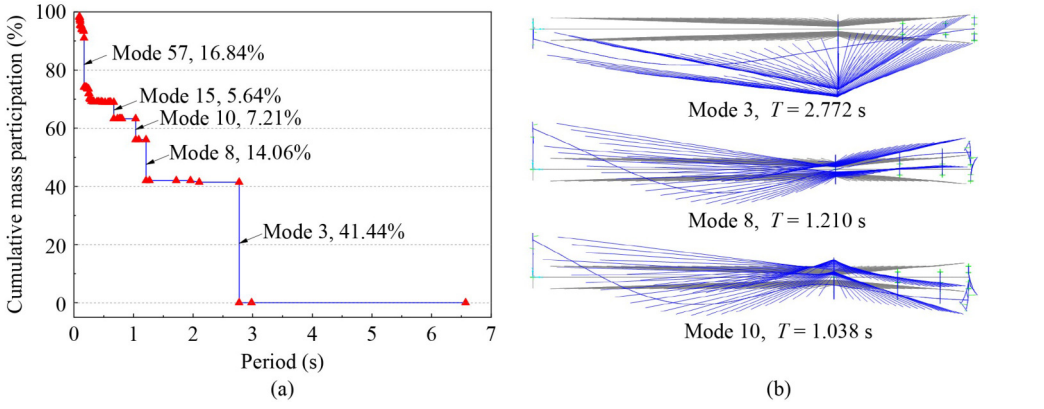

Fig. 6 Structural dynamic characteristics: (a) cumulative mass participation; (b) first three transverse modes in top view.

Table 3 Structural transverse seismic responses

Location	2# Pier	Midspan	3# Tower	4# Pier	5# Pier	6# Pier
Acceleration of girder (*g*)	1.33	0.93	0.65	0.62	0.76	0.88
Shear force of bearing (kN)	11238.4	–	54701.4	2003.9	4712.2	31051.6
Base shear force (kN)	25896.9	–	144140.0	8223.2	13230.5	67373.6

laminated rubber bearing and annular steel wire ropes, demonstrating an inverted S-shaped hysteresis that can be decomposed into an inverted S-shaped elastic link and a coulomb friction. Moreover, the flag-shaped hysteresis obtained from the seismic resilient system that is developed recently can be equivalently simplified as an S-shaped elastic link combined with a coulomb friction [43]. Note that the only difference in the constitutions of the three types of hysteresis lies in the force–displacement path. Therefore, an investigation on the isolation effectiveness of the three types of hysteresis was conducted in this section.

3.1 Method for developing different hysteresis

A multilinear model is proposed to simulate these three types of hysteresis. In this model, a multilinear elastic element is employed to model the linear, S-shaped, and inverted S-shaped constitutive paths. A variable k is defined as the stiffness ratio, i.e., the gradient ratio of the two adjacent line segments of the polyline. Consequently, a linear path is produced with k equal to 1.0, an S-shaped path with k less than 1.0, and an inverted S-shaped path with k larger than 1.0. Subsequently, by connecting an ideal elastoplastic element in parallel with the multilinear elastic element, the expected three types of hysteresis, i.e., the parallelogram-shaped, flag-shaped, and inverted S-shaped hysteresis, can be achieved, as shown in Fig. 8.

Moreover, the model was used to simulate the force-displacement curves of an inverted S-shaped and a flag-shaped energy dissipation systems available in Refs. [42,43], respectively. As can be seen from Fig. 9, the proposed model agrees well with the experimental results, affirming the feasibility of this simulation method.

3.2 Parametric analysis for hysteretic path

Based on the Jinsha River Bridge, a parametric analysis was conducted to investigate the influence of various hysteresis on seismic isolation effectiveness. The stiffness ratio k of the multilinear elastic element was varied from 0.2 to 1.8, with a step of 0.2, to generate a series of hysteresis with different paths of the elastic link. The mechanical parameters of the elastoplastic element remained constant. The number of line segments n of the polyline was set to 10 to achieve a good balance between

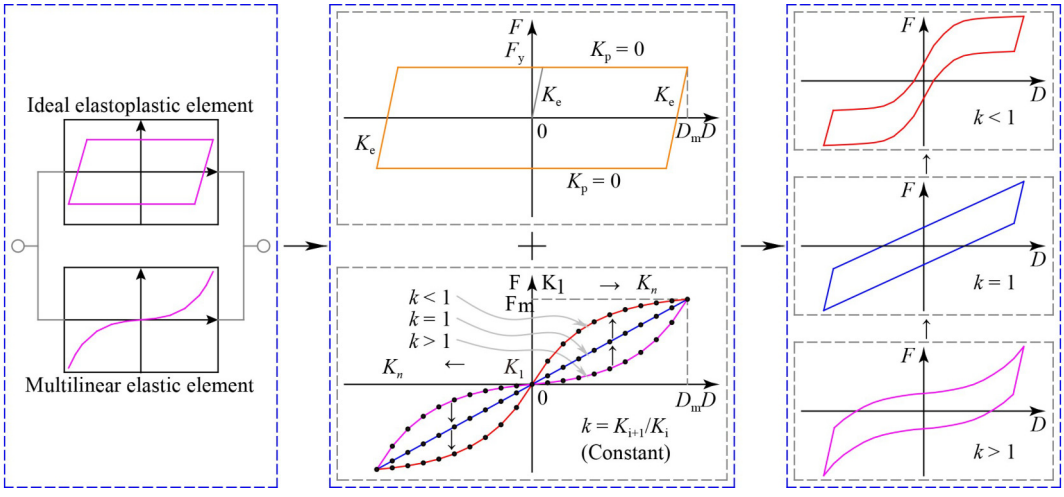

Fig. 8 Schematic diagram of varying the path of hysteretic curve.

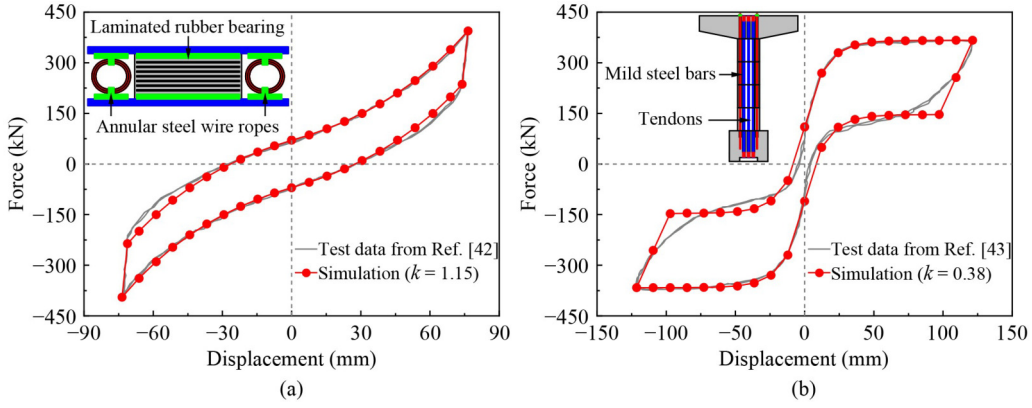

Fig. 9 Experimental validation for the simulation method: (a) inverted S-shaped curve; (b) flag-shaped curve.

computing precision and efficiency. Moreover, two dampers were arranged at each tower/pier position, i.e., ten dampers in total. The dampers at each pier position adopted the same parameters to reflect the difference in their seismic responses caused by structural asymmetry. Considering the great difference in seismic responses between the tower and piers, the stiffness and yield strength of the dampers at the tower position were set to be four times that of the dampers at the pier positions by referring to the lateral shear forces of the bearings at all positions of the lateral fixed system. The specific parameters of the dampers are presented in Table 4. Structural seismic responses with different hysteresis were calculated using nonlinear time-history analysis.

Energy-based approach for seismic behavior analysis provides an effective way of revealing the nature of the dynamic behavior of the structure during earthquakes [27]. The energy equation of a multi-degree-of-freedom structure under the seismic action can be expressed as follows:

$$\int_0^t \{F_a(\ddot{x})\}\mathrm{d}\{x\}^{\mathrm{T}} + \int_0^t \{F_h(\dot{x})\}\mathrm{d}\{x\}^{\mathrm{T}} + \int_0^t \{F_k(x)\}\mathrm{d}\{x\}^{\mathrm{T}} = \int_0^t \{F_e\}\mathrm{d}\{x\}^{\mathrm{T}}, \quad (1)$$

where $\{\ddot{x}\}$, $\{\dot{x}\}$, and $\{x\}$ represent the structural acceleration, velocity, and displacement relative to the ground, respectively; $\{F_a(\ddot{x})\}$, $\{F_h(\dot{x})\}$, $\{F_k(x)\}$, and $\{F_e\}$ represent the inertial force, damping force, elastic force, and earthquake force of each node, respectively. The right side of the equation represents the total input energy of the structure.

Figure 10(a) shows the energy input and dissipation in different isolation systems under the ground motion of ELC270. It is observed that those stiffness ratios k larger than 1.0 tend to result in less input energy and greater energy dissipation compared to those stiffness ratios k less than 1.0. On average, the energy dissipation ratios for stiffness ratios k larger than 1.0 are approximately 54% larger than those for stiffness ratios k less than 1.0. Figure 10(b) presents the detailed cumulative energy input and dissipation of the structure in the isolation systems with stiffness ratios k equal to 0.4 and 1.6. As can be seen from Fig. 10(b), the global input energy for the stiffness ratio k equal to 1.6 (191.31 MJ) is slightly less than that for the stiffness ratio k equal to 0.4 (203.90 MJ). However, the total amount of energy dissipation for the stiffness ratio k equal to 1.6 (72.16 MJ) is significantly larger than that for the stiffness ratio k equal to 0.4 (46.01 MJ). This results in a substantially larger energy dissipation ratio for the stiffness ratio k equal to 1.6 compared to the stiffness ratio k equal to 0.4. Similar results are also observed for other ground motions. These imply that the inverted S-shaped hysteresis could lead to more efficient damping effects.

Figures 11(a) and 11(b) depict the maximum lateral displacements of the dampers and base shear forces of the substructures at different positions, respectively. The responses were averaged across the seven ground motions. As can be seen from Fig. 11(a), those stiffness ratios k less than 1.0 lead to significantly small

Table 4 Mechanical parameters of the dampers

Location	Elastoplastic element				Elastic element			
	D_m (m)	F_y (kN)	K_e (kN/m)	K_p (kN/m)	D_m (m)	F_m (kN)	n	k
Pier	0.5	1000	25000	0	0.5	6000	10	0.2–1.8
Tower	0.5	4000	100000	0	0.5	24000	10	0.2–1.8

Notes: D_m represents the maximum permissible displacement of the damper; F_y, K_e, and K_p represent the yield force, initial elastic stiffness, and post-yield stiffness of the elastoplastic element, respectively; F_m, n, and k represent the maximum permissible force, number of line segments, and stiffness ratio between adjacent line segments of the elastic element, respectively.

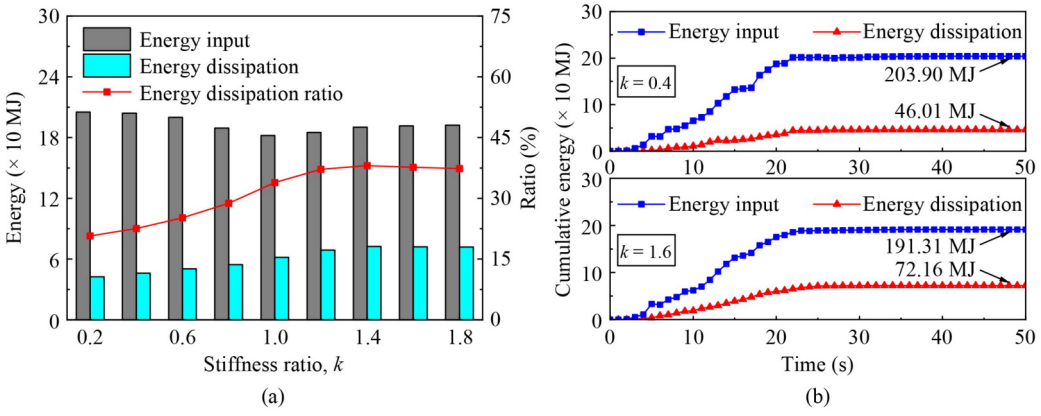

Fig. 10 Energy analysis: (a) energy dissipation ratio of isolation systems; (b) cumulative energy input and dissipation.

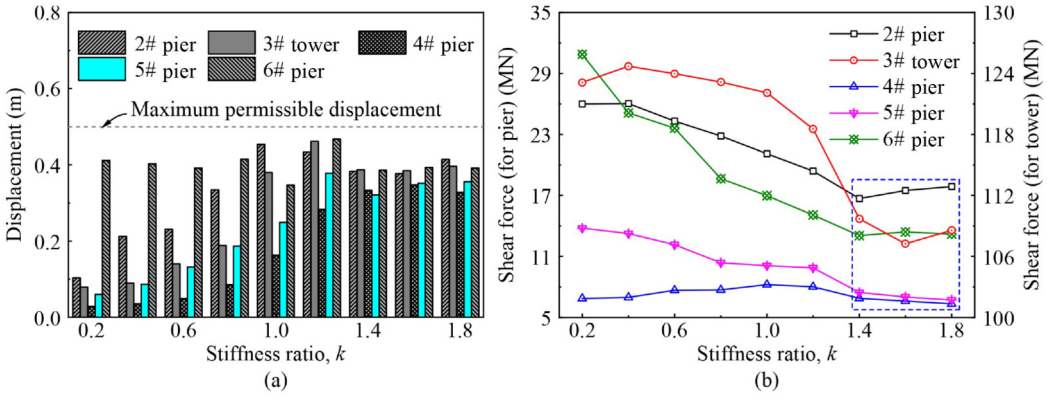

Fig. 11 Seismic responses: (a) maximum lateral displacements of the dampers; (b) maximum base shear forces of the substructures.

displacement responses at all positions except for the 6# pier location, while those stiffness ratios k larger than 1.0 result in basically similar displacement responses at all positions. Furthermore, stiffness ratios k less than 1.0 cause larger base shear forces compared to those stiffness ratios k larger than 1.0, as shown in Fig. 11(b). It can be attributed to the fact that the hysteresis of the dampers with stiffness ratios k larger than 1.0 has relatively smaller secant stiffness compared to those with stiffness ratios k less than 1.0. This could help to balance the great difference in the lateral stiffness of the tower/piers, because the smaller secant stiffness of the dampers governs the overall lateral stiffness in series with the tower/piers. It is also the primary reason for the large displacement responses of the dampers ($k > 1.0$) with minimal differences at various positions, as illustrated in Fig. 11(a). Consequently, the bridge could behave more like a regular structure in terms of the lateral movement of the girder under the seismic action. Moreover, using stiffness ratios k larger than 1.4, the base shear forces of the tower/piers could be decreased to the greatest extent, as shown in Fig. 11(b). These indicate that the inverted S-shaped hysteresis is more suitable for lateral seismic isolation of such a bridge with significant asymmetry.

4 Reasonable damper parameters for lateral isolation system

As mentioned earlier, the wire rope dampers have the expected inverted S-shaped hysteresis. Moreover, these dampers possess a substantial deformation capacity that is crucial for high seismic intensity conditions. In fact, this is why these dampers have been chosen for the lateral seismic isolation of the Jinsha River Bridge. Essentially, a long-span single-tower cable-stayed bridge with significant asymmetry requires an asymmetric arrangement of dampers for the seismic isolation system. This means that the dampers used at different tower/pier locations would have distinct design parameters, and the commonly used exhaustive method for determining these design parameters would be very time-consuming. Therefore, an influence matrix-based method [44] was introduced in this section for determining the reasonable design parameters of dampers in the lateral seismic isolation system.

4.1 Method based on influence matrix

Generally, the force responses of an isolated bridge could be significantly decreased with the use of dampers. However, this may lead to very large relative displacements between the superstructure and substructure, especially in critical seismic conditions [45]. Therefore, the key in designing a lateral isolation system is to control the displacement responses of the dampers, ensuring they do not exceed their deformation capacities [46,47]. Note that the space available between the piers and the girder for installing dampers is similar. Hence, it is convenient and economical to use the same damping units for dampers at different positions, adjusting the required yield force by utilizing different numbers of units combined in parallel. The deformation capacity of the damper is determined by the configuration of the damping unit, which is related to the installation space. Therefore, it is reasonable to set an objective of the same displacement demand for all dampers at different tower/pier locations.

Assuming the initial damping parameters of the dampers at each position of the structure, represented by $\{Q_0\}$, the damping parameters $\{Q_1\}$ of the dampers are calculated according to the differences $\{Z\}$ between the target displacements $\{D_c\}$ of the dampers and their actual displacements $\{D_0\}$ under seismic actions, along with the constructed influence matrix $\{\delta\}$. This process allows the actual displacements $\{D_1\}$ of the dampers corresponding to the damping parameters $\{Q_1\}$ to achieve the magnitude of their target displacements $\{D_c\}$. It should be noted that the seismic response of an actual structural isolation system is a complex nonlinear process, and the influence matrix is not constant. Therefore, several iterations are often required for an accurate calculation. The specific calculation process is illustrated in Fig. 12.

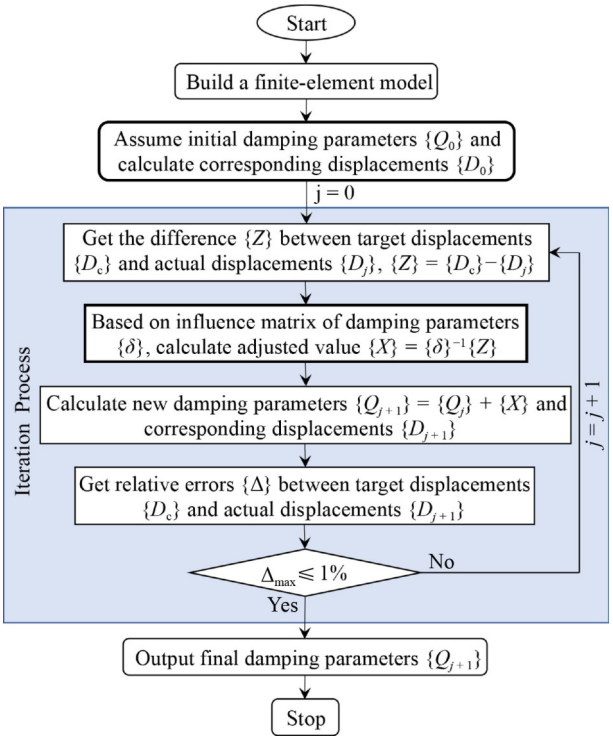

Fig. 12 Calculation process of the influence matrix-based method.

4.2 Reasonable damper parameters of the Jinsha River Bridge

With the influence matrix-based method, the reasonable parameters (yield forces) of wire rope dampers in the lateral isolation system were calculated for the Jinsha River Bridge. As illustrated in Fig. 13, the hysteretic relationship of the wire rope damper was simulated using a multilinear model mentioned in Fig. 8. According to Ref. [42] and the installation space between the girder and the tower/pier, the vital mechanical parameters of the multilinear model for the wire rope damper can be determined. More specifically, the yield displacement D_y of the damper is set to 0.04 m, the ratio of the first post-yield stiffness K_1 to the initial elastic stiffness K_{init} of the damper is taken as 0.151, and the stiffness ratio k between the adjacent post-yield segments (10 segments in total) is equal to 1.2. Moreover, the maximum permissible displacement D_m of the damper is taken as 0.5 m, while the target displacement D_c of the damper is set to 0.45 m for essential safety margin.

Figure 14(a) illustrates the iterative calculation process for determining the reasonable yield forces of the dampers at different tower/pier locations with the displacement objective of 0.45 m. Through six iterations, the desired yield forces of the dampers can be achieved.

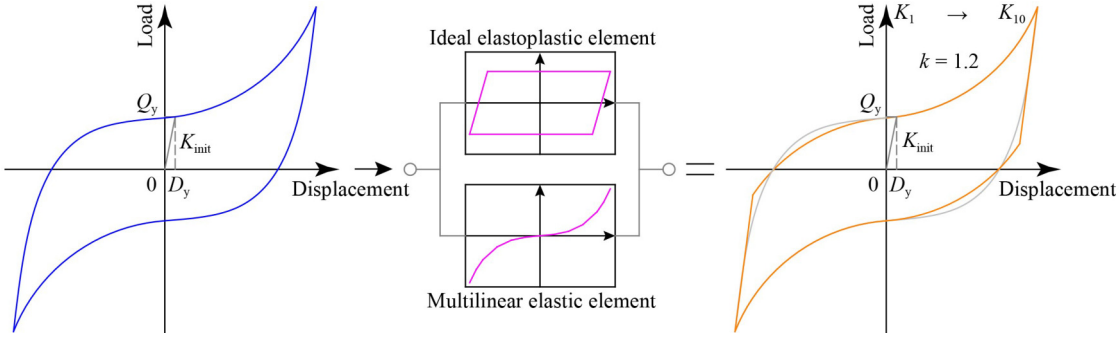

Fig. 13 Simulation method for wire rope damper.

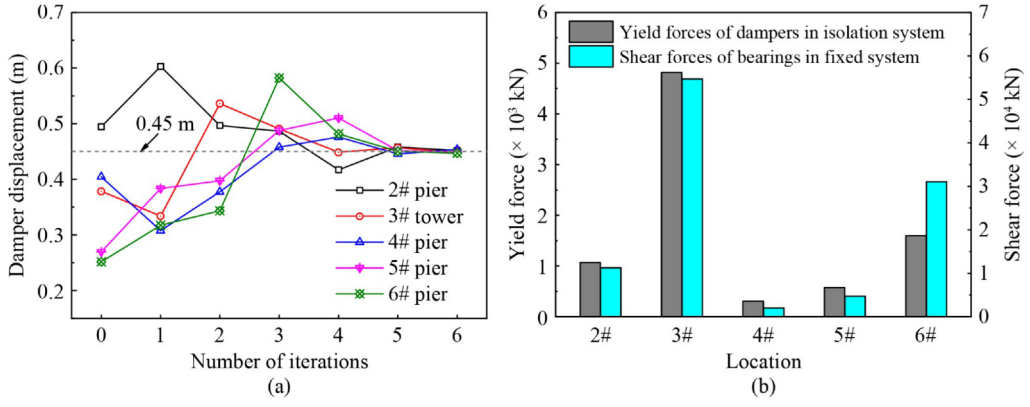

Fig. 14 Iterative process for reasonable yield forces of dampers and corresponding computed result: (a) iterative process; (b) computed result.

This shows the high analytic efficiency of the method. Note that a slight oscillation can be seen in all the curves and all the dampers almost simultaneously reach the target value, indicating the evident interactive effects among the dampers. In fact, it is a generalized method that has a clear concept and high efficiency in iteration and can be used for other asymmetric bridges. As depicted in Fig. 14(b), the reasonable yield forces of the dampers vary significantly at different tower/pier locations. Moreover, the desired yield forces of the dampers are approximately 5% to 15% of the shear forces of the corresponding bearings in the lateral fixed system. This implies that the tower or pier with a larger lateral stiffness requires a larger yield force for the damper.

The previous analysis has shown the dynamic characteristics of the Jinsha River Bridge in the traditional lateral fixed system. As is well known, the introduction of a lateral isolation system will change the structural modal properties [16,25]. Also, the intensity of the seismic load will lead to different level of the structural nonlinearity and thus has influence on the equivalent stiffness of the dampers. Therefore, two modal analyses were conducted for the isolated bridge under 0.5 and 1.0 times the ground motions shown in Fig. 3, respectively. The damping forces and lateral displacements of the dampers at different positions were first calculated through nonlinear time history analyses under the two levels of seismic intensity. Then, the equivalent stiffness of each damper could be calculated for the modal analysis.

Figure 15 depicts transverse modal participating mass ratios of the first 100 modes of the Jinsha River Bridge in the lateral fixed system and the lateral isolation system, as well as the transverse primary mode shapes of the girder in the lateral isolation system. As can be seen from the figure, there are only two modes that contribute significantly to the transverse response of the girder in the lateral isolation system compared to three modes in the lateral fixed system. This indicates that the utilization of wire rope dampers can improve the regularity of the girder to some extent. However, the improvement does not vary significantly with an increase of the nonlinearity of the dampers, since both the periods and mode shapes of the two primary modes do not vary significantly under the two levels of seismic intensity.

5 Influence of geological conditions on reasonable isolation system

5.1 Different terrain conditions

For a single-tower cable-stayed bridge, a typical valley terrain in a mountainous area will inevitably lead to taller piers near the tower and shorter piers away from it. As the

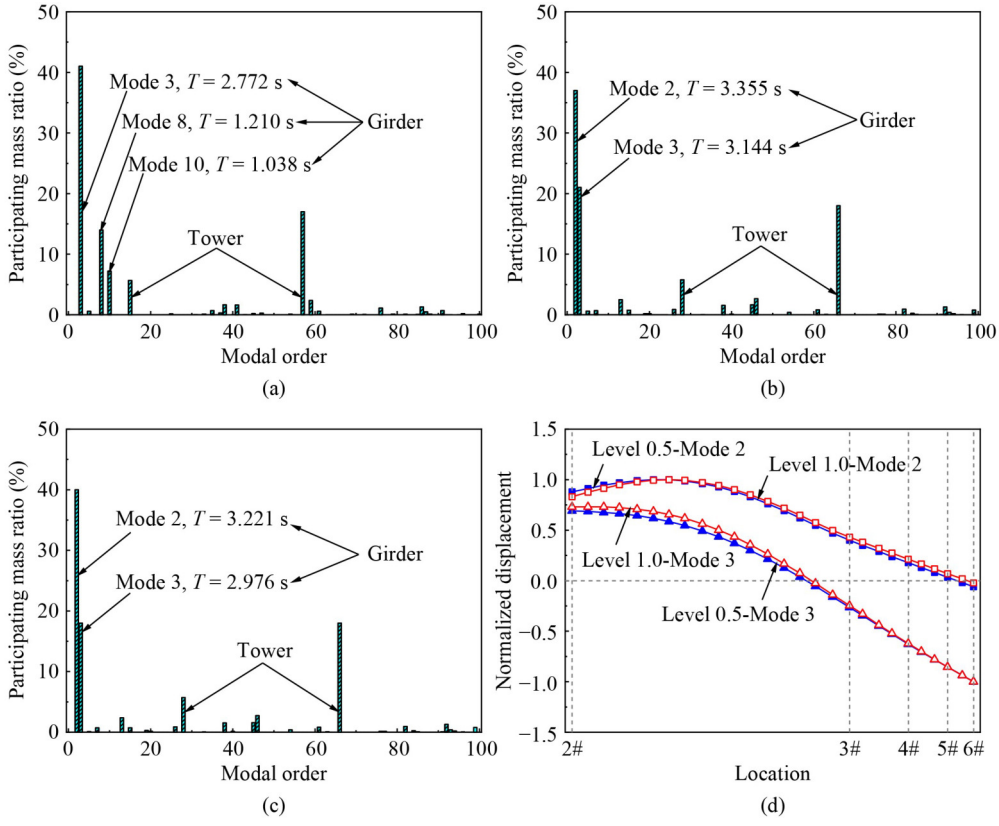

Fig. 15 Modal participating mass ratios of the first 100 modes and primary mode shapes of girder: (a) lateral fixed system; (b) isolation system—level 0.5; (c) isolation system—level 1.0; (d) transverse mode shapes of girder.

distance of the pier from the tower increases, the lateral stiffness of the pier increases significantly. Therefore, the differences in the lateral stiffness of all piers at the side span, which are usually located on the valley slope, are related to the gradient of the valley slope. A steeper slope will lead to larger differences in lateral stiffness of the piers, while a flatter slope could reduce the differences.

To investigate the influence of different gradients of the valley slope on the reasonable design parameters of the dampers for a typical long-span single-tower cable-stayed bridge with a hybrid girder, a parameter sensitivity analysis was conducted on the lateral stiffness of the auxiliary piers (i.e., 4# and 5# piers). Note that the lateral stiffness ratios of the 4# pier to the 5# pier and the 5# pier to the 6# pier of the Jinsha River Bridge are equal to 0.33 and 0.26, respectively, which are both approximately 0.3. Therefore, a relative stiffness ratio for the 4# pier, 5# pier, and 6# pier can be approximately expressed as λ^2: λ: 1, where the smaller value of the λ represents a steeper valley slope and the λ equal to 1.0 means a flat terrain. With a variation of the lateral stiffness ratio λ from 0.1 to 1.0, the ratios of the reasonable yield forces of the dampers in the lateral isolation system to the shear forces of the corresponding bearings in the lateral fixed system were calculated, as shown in Fig. 16(a).

As depicted in Fig. 16(a), the changes in the lateral stiffness of the auxiliary piers have a limited effect on the other piers and the tower, but have a significant effect on themselves. With an increase of the lateral stiffness ratio λ, the ratios of the reasonable yield forces of the dampers at the 4# and 5# auxiliary piers in the lateral isolation system to the shear forces of the corresponding bearings in the lateral fixed system decrease rapidly. When the lateral stiffness ratio λ is equal to 0.1, the ratios of the reasonable yield forces to the bearing shear forces at the 4# and 5# auxiliary piers reach up to 27% and 19%, respectively. Nevertheless, when the lateral stiffness ratio λ is larger than 0.6, the ratios of the reasonable yield forces to the bearing shear forces are about 3% to 10%. Figure 16(b) illustrates the specific distributions of the reasonable yield forces and the bearing shear forces at λ = 0.6. The correlation between the reasonable yield forces of the dampers and the shear forces of the bearings in the lateral fixed system is shown again. This implies that a primary estimation of the reasonable yield forces of the dampers could be based on the shear forces of the corresponding bearings in the lateral fixed system that could be easily calculated with a linear model, especially for those with λ larger than 0.6.

However, a significant disparity in the design parameters for dampers at different tower/pier locations in an isolation system would cause difficulty and inconvenience in design, fabrication, and maintenance of the dampers. Alternatively, an approximate and more practical design might be that those dampers with small yield forces could be removed from the lateral isolation system.

Figure 17(a) shows the relative displacements between the tower/piers and the girder for different lateral stiffness ratios λ with free constraints at the auxiliary piers. It can be observed from the figure that the absence of dampers at the auxiliary piers has a significant impact on their own relative displacements between the piers and the girder. As the lateral stiffness ratio λ increases from 0.1 to 0.6, the relative displacements at the auxiliary piers decrease rapidly, reducing from 0.86 to 0.59 m for the 4# pier and from 0.73 to 0.55 m for the 5# pier. When the lateral stiffness ratio λ is greater than 0.6, the vibration of the relative displacements at the auxiliary piers becomes negligible, not exceeding 7%. In Fig. 17(b), the displacement time histories of the pier top and the girder at the 4# pier location under the ground motion of ELC270 are presented, with the lateral stiffness ratio λ equal to 0.1 and 0.6, respectively. Similar results are also observed for other ground motions. It can be seen that the displacements of the girder at the 4# pier are nearly the same for different lateral stiffness ratios, with the maximum displacements around 0.46 m. However, the

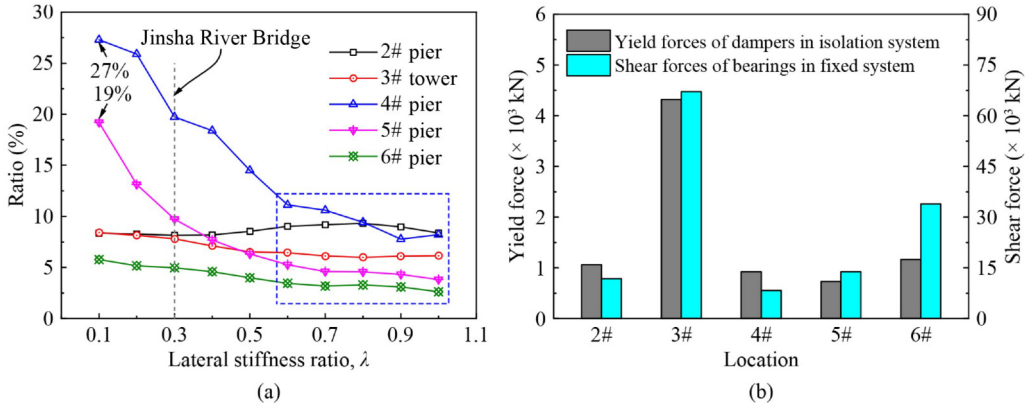

Fig. 16 Comparison of reasonable damper yield forces and fixed bearing shear forces: (a) ratios of yield forces to shear forces; (b) yield forces and shear forces at λ = 0.6.

displacements of the pier top are quite different. For the lateral stiffness ratio λ equal to 0.1, the maximum displacement at the top of the 4# pier is approximately 0.84 m, much larger than the displacement of the girder. Nevertheless, for the lateral stiffness ratio λ equal to 0.6, the displacement of the pier top is only about 0.07 m, considerably smaller than the displacement of the girder. These indicate that for small lateral stiffness ratios λ, the displacements of the auxiliary pier tops would be larger than those of the girder due to the small lateral stiffness of the piers. As a result, the necessary damper installed between the auxiliary pier and the girder is not to restrain the displacement of the girder by the pier, but to restrain the displacement of the pier top by the girder. This also well explains the phenomenon that the ratios of the reasonable yield forces of the dampers at the auxiliary piers in the lateral isolation system to the shear forces of the corresponding bearings in the lateral fixed system are greatly large when the lateral stiffness ratio λ is small (as seen in Fig. 16(a)).

Figures 18(a) and 18(b) depict the normalized base shear forces of the tower/piers in the two lateral isolation systems mentioned above. As can be seen from the figures, the damping effects on the 2# pier and the 3# tower in the two lateral isolation systems with various lateral stiffness ratios λ are similar. This is because the 2# pier is far away from the auxiliary piers, and the base shear force of the 3# tower is contributed not only by the shear force transferred from the girder but also by its own inertia force. The damping effect on the 6# pier is much better than that on the 2# pier and 3# tower, especially in the system using dampers at the auxiliary piers. This is because the large inertia force of the massive concrete girder at the side span is mainly transferred to the 6# pier that has a relatively larger lateral stiffness. Moreover, both lateral isolation systems exhibit low damping effects on the 4# and 5# auxiliary piers at small lateral stiffness ratios λ and high damping effects at large lateral stiffness ratios λ. For some small lateral stiffness ratios λ, the shear force ratios could even exceed 1.0 in both lateral isolation systems, especially in the system without dampers employed at the auxiliary piers, which means the base shear forces of the auxiliary piers in the lateral isolation system are larger than those in the lateral fixed system. This is consistent with the phenomenon (as shown in Fig. 17(b)) that significantly low lateral stiffness of the auxiliary piers would result in much larger displacement responses at the pier tops compared to those

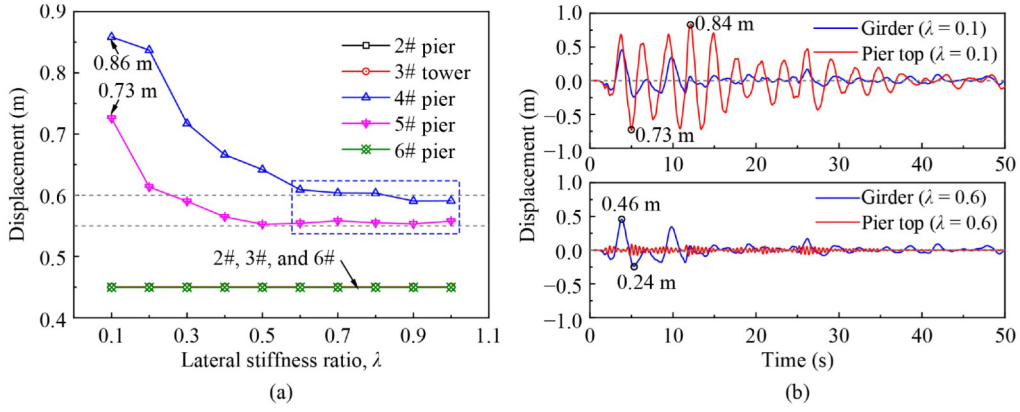

Fig. 17 Displacement responses for different relative stiffness of auxiliary piers without dampers: (a) pier/tower-girder relative displacements; (b) displacement time histories at the 4# pier.

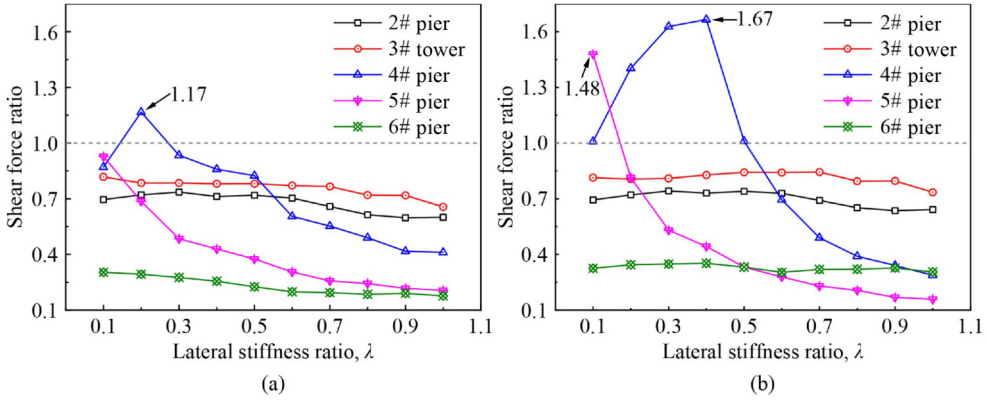

Fig. 18 Ratios of base shear forces of tower/piers in two isolation systems to those in fixed system: (a) isolation system with dampers at auxiliary piers; (b) isolation system without dampers at auxiliary piers.

of the girder, necessitating the use of dampers at the auxiliary piers to control the seismic responses of the auxiliary piers themselves.

From the above analysis, it can be concluded that for such a long-span single-tower cable-stayed bridge with a hybrid girder, when the side span crosses a steep valley slope, it would be reasonable to install dampers at all positions. This can help to control the relative displacements between the girder and the tower/piers, as well as reduce the base shear forces of the tower/piers. However, when the side span crosses a gentle valley slope, a lateral isolation system without dampers at the auxiliary piers could be employed, which also exhibits an excellent damping effect.

5.2 Different site conditions

As is known, structural seismic responses are significantly influenced by the frequency content of ground motions that are related to local site conditions [16]. This section aims to investigate the influence of different site conditions on the reasonable lateral seismic isolation system for such a long-span single-tower cable-stayed bridge in mountainous areas.

In the code JTG/T 2231-01-2020 [38], five types (I_0–IV) of sites are categorized based on the local soil conditions, and each type of site is associated with a different characteristic period ranging from 0.2 to 0.9 s. Moreover, different site coefficients ranging from 0.76 to 1.00 are used to adjust the design PGA. Therefore, a set of response spectra with various characteristic periods and site coefficients were developed to investigate the influence of different site types. More specifically, the variation of the characteristic period was quantified by a uniform distribution, as shown in Fig. 19(a). One artificial acceleration time history was randomly generated for each response spectrum. Figure 19(b) depicts two representative acceleration time histories with characteristic periods equal to 0.303 and 0.821 s, respectively. Finally, 200 numerical analysis cases based on the Jinsha River Bridge with different site conditions were carried out.

Figure 20(a) illustrates the reasonable yield forces of the dampers at each tower/pier location of the Jinsha River Bridge under excitations with different characteristic periods. It can be observed that the reasonable damper yield forces generally increase with an increase of the characteristic period. Specifically, when the characteristic period is less than 0.35 s, the reasonable yield forces of the dampers are equal to 0. This is because

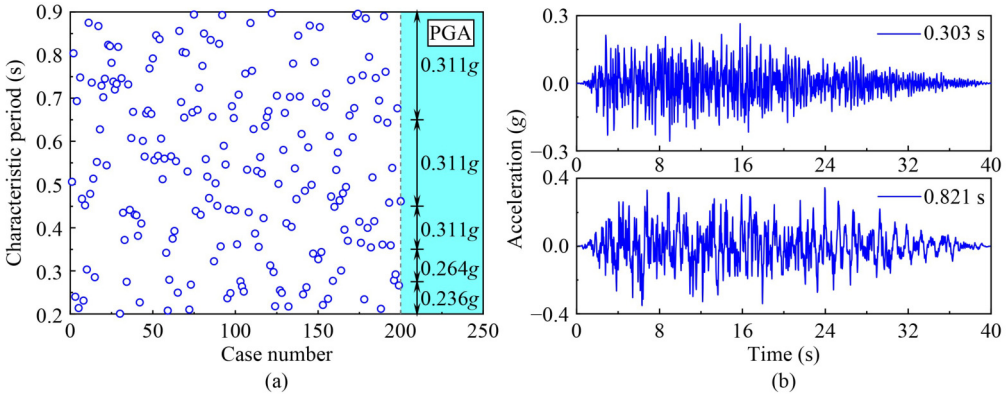

Fig. 19 Statistical distribution of the characteristic period and two representative time histories: (a) scatterplot of characteristic period; (b) acceleration time histories.

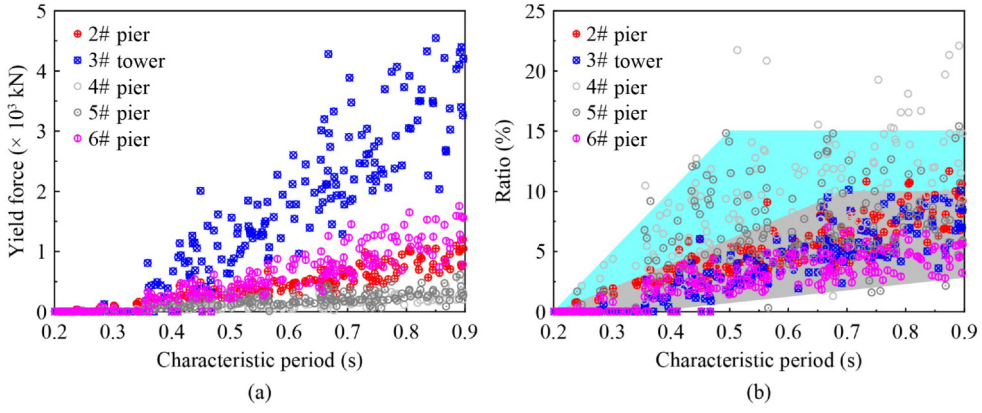

Fig. 20 Reasonable damper yield forces and ratios of reasonable damper yield forces to fixed bearing shear forces for different characteristic periods: (a) reasonable damper yield forces; (b) ratios of yield forces to shear forces.

the damper displacements have not exceeded the target displacement of 0.45 m. For the characteristic period larger than 0.35 s, the maximum yield forces of the dampers are expected at the tower and the smallest at the auxiliary piers, which is consistent with the phenomenon shown in Fig. 14(b). When compared to the lateral fixed system, as shown in Fig. 20(b), the reasonable yield forces of the dampers at the 2# pier, 3# tower, and 6# pier are about 2% to 10% of the shear forces of the corresponding bearings in the lateral fixed system, while those at the 4# and 5# auxiliary piers are about 2% to 25% with a large dispersion. This is because the shear forces of the bearings at the 4# and 5# auxiliary pier locations in the lateral fixed system are relatively small due to the small lateral stiffness of the piers and are also significantly influenced by high-order modes. The results illustrate again the correlation between the reasonable yield forces of the dampers in the lateral isolation system and the shear forces of the corresponding bearings in the lateral fixed system.

Figure 21 displays the maximum base shear forces of the tower/piers in the lateral isolation system with the reasonable damper yield forces for different characteristic periods. It exhibits that the base shear forces at all positions show an overall increasing trend with an increase of the characteristic period. This is because the larger the characteristic period, the wider the frequency band rich in seismic energy, which is more likely to cause greater seismic responses in long-period structures, similar to structural resonance [48,49]. It should be noted that due to the damper nonlinearity, the stiffness and the period of the isolated bridge vary continually with an increase of the deformation of the dampers under the seismic action, and thus such resonance behavior is much more complicated than that with constant structural stiffness and mode periods.

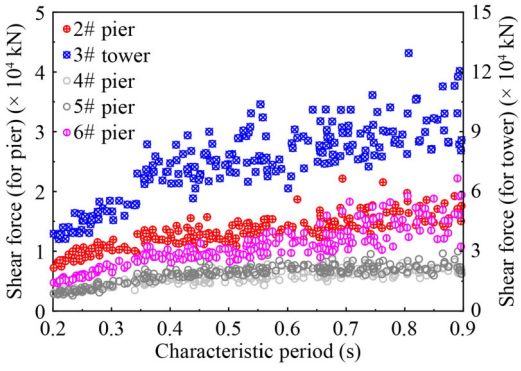

Fig. 21 Base shear forces of tower/piers in isolation system for different characteristic periods.

6 Conclusions

This paper aims to develop a reasonable lateral seismic isolation system for a typical long-span single-tower cable-stayed bridge with a hybrid girder that is particularly suitable for the mountainous areas in central and western China with high seismic risk. Based on the Jinsha River Bridge, the significant structural asymmetry and its effects on structural seismic responses were analyzed. Then, a parametric analysis was conducted to investigate the appropriate damping hysteresis for lateral seismic isolation of the bridge, and an influence matrix-based method was used to calculate the reasonable design parameters of dampers. Moreover, the influences of geological conditions including different terrain and site conditions on the reasonable lateral isolation system of the bridge were further discussed. The main conclusions are as follows.

1) The typical long-span single-tower cable-stayed bridge with a hybrid girder has significant asymmetry in span arrangement, mass distribution, and lateral stiffness of the tower/piers, resulting in a highly intricate dynamic behavior in seismic conditions. The lateral seismic responses of this cable-stayed bridge are governed by multiple modes.

2) The inverted S-shaped hysteresis is more suitable for lateral seismic isolation of such a bridge with significant asymmetry because the relatively smaller secant stiffness of the inverted S-shaped hysteresis could help to balance the great difference in the lateral stiffness of the tower/piers. The inverted S-shaped hysteresis could lead to more efficient damping effects and less base shear forces of the tower/piers.

3) The reasonable parameters of the dampers at different tower/pier locations can be efficiently calculated by the influence matrix-based method. There is a correlation between the reasonable yield forces of dampers in the lateral isolation system and the shear forces of bearings in the lateral fixed system, which is observed in both soft and hard site conditions. Soft sites require larger damper yield forces and cause greater seismic responses compared to hard sites.

4) When the side span of such a single-tower cable-stayed bridge with a significantly asymmetric span arrangement crosses a steep valley slope, it would be reasonable to use dampers at all tower/pier locations, while the side span of the bridge crosses a gentle valley slope, a lateral isolation system without using dampers at the auxiliary piers could be employed.

Acknowledgements This work was supported by the National Natural Science Foundation of China (Grant No. 52278527). The authors gratefully acknowledge the anonymous reviewers who have contributed to essentially improving the paper. Any opinions, findings, and conclusions expressed are those of the authors and do not necessarily reflect those of the sponsoring organizations.

Competing interests The authors declare that they have no competing interests.

References

1. Guan Z, Li J. Advances in earthquake resisting systems for long-span bridges. Scientia Sinica (Technologica), 2021, 51(5): 493–504 (in Chinese)
2. Xie W, Sun L. Transverse failure modes and control strategies of super long-span cable-stayed bridge under extreme earthquake. Journal of Vibroengineering, 2017, 19(8): 6152–6169
3. Bauer K W, Wilson J R. Control-variate selection criteria. Naval Research Logistics, 1992, 39(3): 307–321
4. Xu X, Liu W, Li L, Li S, Fang H. Optimized earthquake reduction design of cable-stayed bridges. Earthquake Engineering and Engineering Dynamics, 2006, 26(2): 119–124 (in Chinese)
5. Ye A, Fan L. Lateral constraint systems for super-long-span cable-stayed bridge. China Journal of Highway and Transport, 2007, 20(2): 63–67 (in Chinese)
6. Hamby D M. A review of techniques for parameter sensitivity analysis of environmental-models. Environmental Monitoring and Assessment, 1994, 32(2): 135–154
7. Shen Y, Li J, Freddi F, Igarashi A, Zhou J. Numerical investigation of transverse steel damper (TSD) seismic system for suspension bridges considering pounding between girder and towers. Soil Dynamics and Earthquake Engineering, 2022, 155: 107203
8. Zhou L, Shahria Alam M, Song A, Ye A. Probability-based residual displacement estimation of unbonded laminated rubber bearing supported highway bridges retrofitted with transverse steel damper. Engineering Structures, 2022, 272: 115053
9. Jiang L, Yan Y, Wen T, Jiang L, Yu K, Pang L. System-level seismic fragility of high-speed railway track-bridge system with component-replaceable U-shaped combined steel damper. Structures, 2023, 58: 105452
10. Guan Z, Li J, Xu Y. Performance test of energy dissipation bearing and its application in seismic control of a long-span bridge. Journal of Bridge Engineering, 2010, 15(6): 622–630
11. Cai X, Zhu Y, Wang J, Wang P, Wen Y. Seismic behavior of self-centering precast segmental bridge piers with external auxetic steel shear panel dampers. Structures, 2023, 58: 105647
12. Liu M, Gao H, Wang J, Dong Z, Yan H. Earthquake damage index and fragility analysis of steel damper for seismic isolation bridge. Applied Sciences-Basel, 2023, 13(12): 7095
13. Camara A, Astiz M A. Analysis and control of cable-stayed bridges subject to seismic action. Structural Engineering International, 2014, 24(1): 27–36
14. Camara A, Cristantielli R, Astiz M A, Málaga-Chuquitaype C. Design of hysteretic dampers with optimal ductility for the transverse seismic control of cable-stayed bridges. Earthquake Engineering & Structural Dynamics, 2017, 46(11): 1811–1833
15. Shen X, Ni X, Ye A. A new type of metallic damper for bridges' aseismic performance in transverse direction. Journal of Vibration and Shock, 2014, 33(21): 96–101 (in Chinese)
16. Shen X, Ni X, Ye A. Seismic system and design method of transverse metallic yielding dampers on long-span cable-stayed bridge side piers. China Civil Engineering Journal, 2016, 49(5): 110–119 (in Chinese)
17. Shen X, Wang X, Ye Q, Ye A. Seismic performance of transverse steel damper seismic system for long span bridges. Engineering Structures, 2017, 141: 14–28
18. Burcsi P, Kovacs A. Exhaustive search methods for CNS polynomials. Monatshefte für Mathematik, 2008, 155(3–4): 421–430
19. Xu Y, Zeng S. Study of optimal seismic mitigation of steel dampers arranged on cable-stayed bridge in transverse bridge direction. Bridge Construction, 2017, 47(3): 53–58 (in Chinese)
20. Xu Y, Zeng Z, Cui C, Zeng S. Practical design method of yielding steel dampers in concrete cable-stayed bridges. Applied Sciences-Basel, 2019, 9(14): 2857
21. Wen J, Han Q, Xie Y, Du X, Zhang J. Performance-based seismic design and optimization of damper devices for cable-stayed bridge. Engineering Structures, 2021, 237: 112043
22. Niu J, Ding Y, Shi Y, Li Z. A simplified design method for metallic dampers used in the transverse direction of cable-stayed bridges. Earthquake Engineering and Engineering Vibration, 2020, 19(2): 483–497
23. He X, Zhang J, Fan C, Yang Y, Xiao X. Study of transverse seismic system for Xigu Huanghe River Bridge in Lanzhou. Bridge Construction, 2018, 48(1): 65–70 (in Chinese)
24. Wang H, Shen W, He T, Huang M, Zhu H. Optimal seismic mitigation of transverse C-shaped steel damper of two series-connected long-span cable-stayed bridges. Journal of Civil Engineering and Management, 2021, 38(4): 133–139 (in Chinese)
25. Guan Z, You H, Li J. Lateral isolation system of a long-span cable-stayed bridge with heavyweight concrete girder in a high seismic region. Journal of Bridge Engineering, 2017, 22(1): 4016104
26. Guan Z, You H, Guo H. Responses of cable-stayed bridge transversely isolated with elastoplastic cable pairs and fluid viscous damper subjected to near fault ground motions. Journal of Tongji University (Natural Science), 2016, 44(11): 1653–1659 (in Chinese)
27. Guan Z, You H, Li J. An effective lateral earthquake-resisting system for long-span cable-stayed bridges against near-fault earthquakes. Engineering Structures, 2019, 196: 109345
28. You H, Guan Z. Elastoplastic cable pair and viscous damper used in the lateral seismic isolation of cable-stayed bridges. Journal of Vibration and Shock, 2017, 36(14): 183–188 (in Chinese)
29. Guan Z, Li J, Qu H. Shake table test and numerical study on a capable and resilient lateral seismic isolation system for long-span cable-stayed bridges. Soil Dynamics and Earthquake Engineering, 2023, 164: 107629
30. Guo J, Li M, Wu Y, Xiao Y, Guan Z. Experimental study on a cable-stayed bridge isolated with the combination of elastoplastic cables and fluid viscous dampers in the transverse direction. Engineering Structures, 2024, 302: 117447
31. Ancheta T D, Darragh R B, Stewart J P, Seyhan E, Silva W J, Chiou B S J, Wooddell K E, Graves R W, Kottke A R, Boore D M, et al. NGA-West2 database. Earthquake Spectra, 2014, 30(3): 989–1005
32. Xu Y, Cui C, Zeng Z, Zeng S. Shake table experimental study of cable-stayed bridges with two different design strategies of H-shaped towers. Earthquake Engineering and Engineering Vibration, 2021, 20(2): 483–493
33. Xie W, Sun L, Lou M. Shaking table test verification of traveling

wave resonance in seismic response of pile-soil-cable-stayed bridge under non-uniform sine wave excitation. Soil Dynamics and Earthquake Engineering, 2020, 134: 106151
34. Thai H T, Kim S E. Second-order inelastic analysis of cable-stayed bridges. Finite Elements in Analysis and Design, 2012, 53: 48–55
35. Shi Z, Dimitrakopoulos E G. Nonsmooth dynamics prediction of measured bridge response involving deck-abutment pounding. Earthquake Engineering & Structural Dynamics, 2017, 46(9): 1431–1452
36. Hinrichs N, Oestreich M, Popp K. Dynamics of oscillators with impact and friction. Chaos, Solitons and Fractals, 1997, 8(4): 535–558
37. JTG 3363-2019. Specifications for Design of Foundation of Highway Bridges and Culverts. Beijing: Ministry of Transport of the People's Republic of China, 2019 (in Chinese)
38. JTG/T 2231-01-2020. Specifications for Seismic Design of Highway Bridges. Beijing: Ministry of Transport of the People's Republic of China, 2020 (in Chinese)
39. Mokha A, Constantinou M C, Reinhorn A M, Zayas V A. Experimental study of friction-pendulum isolation system. Journal of Structural Engineering, 1991, 117(4): 1201–1217
40. Tsopelas P, Constantinou M C, Kim Y S, Okamoto S. Experimental study of FPS system in bridge seismic isolation. Earthquake Engineering & Structural Dynamics, 1996, 25(1): 65–78
41. Fenz D M, Constantinou M C. Behaviour of the double concave friction pendulum bearing. Earthquake Engineering & Structural Dynamics, 2006, 35(11): 1403–1424
42. Wan X, Hou H, Wan W, Xiong S. Study on the mechanical properties of the laminated rubber isolation bearing with annular steel wire ropes. Journal of Wuhan University of Technology, 2016, 38(5): 64–69 (in Chinese)
43. Ou Y C, Wang P H, Tsai M S, Chang K C, Lee G C. Large-scale experimental study of precast segmental unbonded posttensioned concrete bridge columns for seismic regions. Journal of Structural Engineering, 2010, 136(3): 255–264
44. Zhang S, Guan Z. Reasonable transverse isolation system for long-span single-tower cable-stayed bridges with hybrid girders in mountainous areas. Journal of Basic Science and Engineering, 2024, 32(1): 258–272 (in Chinese)
45. Dicleli M. Performance of seismic-isolated bridges in relation to near-fault ground-motion and characteristics. Earthquake Spectra, 2006, 22(4): 887–907
46. Dimitrakopoulos E, Makris N, Kappos A J. Dimensional analysis of the earthquake-induced pounding between adjacent structures. Earthquake Engineering & Structural Dynamics, 2009, 38(7): 867–886
47. Jónsson M H, Bessason B, Haflidason E. Earthquake response of a base-isolated bridge subjected to strong near-fault ground motion. Soil Dynamics and Earthquake Engineering, 2010, 30(6): 447–455
48. Benedettini F, Rega G, Alaggio R. Nonlinear oscillations of a four-degree-of-freedom model of a suspended cable under multiple internal resonance conditions. Journal of Sound and Vibration, 1995, 182(5): 775–798
49. Kang H, Guo T, Zhu W. Analysis on in-plane 2:2:1 internal resonance of a complex cable-stayed bridge system under external harmonic excitation. Journal of Computational and Nonlinear Dynamics, 2021, 16(10): 101001